Preprint version of:
Suarez, A., Jimenez-Cano, A. E., Vega, V. M., Heredia, G., Rodríguez-Castaño, A., & Ollero, A. (2017, June). Lightweight and human-size dual arm aerial manipulator. In 2017 International Conference on Unmanned Aircraft Systems (ICUAS) (pp. 1778-1784).

Lightweight and Human-size Dual Arm Aerial Manipulator

A. Suarez, A. E. Jimenez-Cano, V. M. Vega, G. Heredia, A. Rodriguez-Castaño and A. Ollero

***Abstract*—This paper presents the design of a dual-arm aerial manipulator consisting of a multi-rotor platform with an ultra-lightweight (1.8 Kg) human-size dual arm prototype and its control system. Each arm provides three degrees of freedom (DOF) for positioning the end-effector, and two DOF for orientation. As most model-based controllers assume that joint torque feedback is available, a torque estimator for the arms is developed. Note that low cost servos used for building low weight manipulators do not provide any torque feedback or control capability. The redundant DOFs in the dual arm prototype are exploited for generating coordinated motions during contact-less phases in such a way that reaction torques can be partially canceled. Preliminary flight tests have been conducted in outdoors, evaluating the torque compensation capability in test-bench. The influence of the reaction torques exerted by the arms over the UAV controller is also analyzed in simulation.**

I. Introduction

Aerial manipulation with VTOL (Vertical Take-Off and Landing) UAVs (Unmanned Aerial Vehicles) is becoming a field of interest in recent years motivated by the possibility of performing certain manipulation tasks in places of difficult access such like bridges, wind turbine generators and other industrial facilities, integrating one or more robotic arms in aerial vehicles such like autonomous helicopters [1] or multi-rotors [2]. However, the control of an aerial manipulation system is a hard task due to the strong dynamic coupling between the arms and the aerial platform [3][4][5], in the sense that any motion of the arms generates a reaction torque supported by the aerial vehicle that causes a perturbation in its attitude and position. What is more, in those applications or tasks involving interactions with the environment like load grasping [6] or valve turning [7], the aerial manipulator will also be affected by external forces propagated from the robotic arm to the base of the aerial platform [8]. In order to control this perturbation, it is highly desirable to have a method for estimating the torque generated by the arms so it can be compensated [9][10]. Momentum based methods are applied in [11][12] for estimating external forces and torques as well as unmodeled dynamics in a quadrotor UAV, although these methods are only suitable to compensate slow motions.

Torque compensation with multiple robot manipulators has been already documented in space applications. Dual arm coordination is considered in [13] for minimizing the total operation torque of a satellite with two robotic manipulators, one used for the execution of the grasping operation, while the other compensates the torque generated by the later. Torque optimization control exploiting the redundancy in a space free-floating robot equipped with multiple manipulators is explored in [14]. References [15][16] consider the concept of Virtual Manipulator for expressing the dynamic equations of this kind of systems in a more convenient form.

Several platforms and aerial manipulation prototypes have been documented in more recent works. Torque compensation with a quadrotor platform equipped with two small grasping manipulators is demonstrated in [17]. A 7-DoF industrial manipulator integrated in an autonomous helicopter is shown in [18]. The mechanical design of low weight robotic arms for multirotor platforms are detailed in [19][20]. Joint compliance in lightweight, human-size robotic arm has been exploited for payload estimation [21], contact force control and collision detection [22]. Two 2-DOF arms acting as grippers are employed in [7] for the valve turn operation. Recently a large hexarotor platform equipped with two arms has been presented for object transportation [23].

The main contribution of this paper is the development of a dual arm aerial manipulation system consisting of an ultra-lightweight (1.8 Kg weight) and low inertia, human-size dual arm prototype [24] integrated in a multirotor platform (Figure 1). The arms are said to be ultra-lightweight for remarking the difference with respect to lightweight industrial robots which are one order of magnitude heavier (around 20 Kg each arm). Motivated by the convenience of compensating the reaction torques that the arms exert over the UAV, and taking into account that most servo actuators used for building low weight robotic arms do not provide any torque feedback, a torque estimator is designed along with the control system of the aerial robot. Preliminary flight tests have been conducted in outdoors for evaluating qualitatively the influence of arms motion over the multi-rotor platform, and, in particular, the coordination of left and right arms for reducing the oscillations in the roll and yaw angles. Simulation results evidence that the performance in the position control of the aerial manipulator is enhanced when the estimator is applied for the compensation.

Figure 1. Dual arm aerial manipulation system consisting in two 5-DOF human size arms integrated in an octo-rotor platform.

A. Suarez (e-mail: asuarezfm@us.es), A. E. Jimenez-Cano (email: antenr@hotmail.com), G. Heredia (e-mail: guiller@us.es), V. M. Vega (email: victorvegaes@gmail.com), A. Rodriguez-Castaño (email: castano@us.es) and A. Ollero (e-mail: aollero@us.es) are with the Robotics, Vision and Control Group at University of Seville, Spain.

The rest of the paper is organized as follows. Section II describes the dual arm aerial manipulation system, including the dual arm system design, the multirotor platform, and the electronics and software. Section III covers the modeling and control, while Section IV describes the developed estimator. The results of this work are shown in Section V, presenting the conclusion in Section VI.

II. Dual Arm Aerial Manipulation System

A. Dual Arm System

The dual arm system consists in two human size arms, left and right, built with the Herkulex smart servos and a set of fifty two anodized aluminum frames manufactured by hand from 20x2 and 30x2 flat, and 8 mm Ø hollow circular profiles. Each arm, weighting 800 grams, provides 5-DoF: shoulder yaw, shoulder pitch and elbow pitch for end-effector positioning, and, wrist roll and pitch for orientation. However, this work only considers the positioning joints in the dynamic model, as the mass and inertia of the orientation joints is not significant. A rendered view of the developed dual arm system with its dimension and the weight of the actuators has been depicted in Figure 2, summarizing its main specifications on Table 1 and Table 2. The proposed kinematic configuration (shoulder yaw joint at the base followed by the shoulder pitch and elbow pitch joints), maximizes the volume of operation of each arm, and at the same time simplifies the equations of the kinematic model.

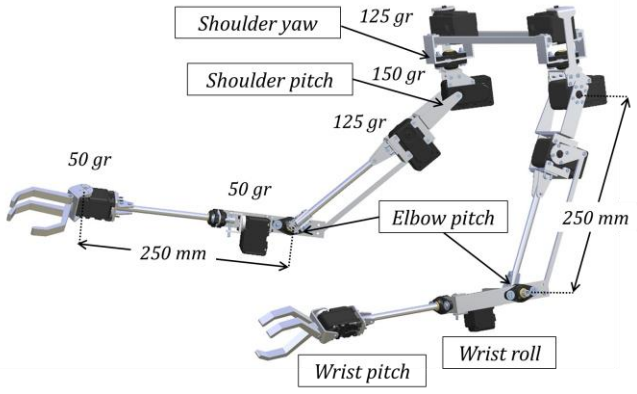

Figure 2. Rendered view of the lightweight dual arm system with its dimensions and the actuators weight. The elbow pitch servo has been placed under the shoulder pitch servo, using a rigid bar for motion transmission

Table 1. Specifications of the lightweight dual arm manipulator.

Weight	Actuators: 1 Kg Frame: 0.8 Kg Total: 1.8 Kg
Max. lift load per arm	~0.75 Kg
Dimensions	Upper arm: 0.25 m Forearm: 0.25 m Arms separation: 0.25 m
Volume of operation	0.255 m^3 (each arm)
Actuators	Herkulex Smart Servos
Kinematic configuration	Shoulder yaw – Shoulder pitch, Elbow pitch – Wrist roll – Wrist pitch
Power source	3S, 5000 mAh LiPo battery

Table 2. Specifications of each joint in the dual arm manipulator.

Joint	Servo model	Torque [N·m]	Rotation range [deg]
Shoulder yaw	DRS-0402	5,1	[-90, +90]
Shoulder pitch	DRS-0602	7,6	[-90, +90]
Elbow pitch	DRS-0402	5,1	[10, 160]
Wrist roll	DRS-0101	1,17	±150
Wrist pitch	DRS-0101	1,17	±150

The arms have been specifically designed for research in aerial manipulation, which imposes severe constraints due to payload limitation and dynamic coupling with the aerial platform. For that reason, most part of the mass of the actuators has been displaced as far as possible to the top of the links in order to reduce the inertia. As seen in Figure 2, the elbow pitch servo is immediately under the shoulder pitch servo, and the wrist roll actuator is close to the elbow pitch shaft. What is more, the slim design of the frame structure of the arms has a low impact on the aerodynamics of the multi-rotor platform. The actuators employed in the development of the arms were the Herkulex smart servos due to their very high torque to weight ratio and because they include the motor, gearbox, electronics, communications and control in a compact device that can be easily assembled with the other frame parts.

B. Multirotor Platform

A picture of the developed dual arm aerial manipulator is shown in Figure 1. The aerial platform is a quadrotor in coaxial configuration, a 30 cm height landing gear and a central body in carbon fiber containing all the electronics. The batteries are located at the back of the central body for compensating the displacement of the center of gravity due to the dual arm system. The total weight of the system is around 9 Kg, with a flight autonomy around 10 min when powered with a LiPo 5S, 10000 mAh battery. The placement of the arms is constrained by the landing gear and the frame structure of the central hub. As it can be seen in Figure 1, the arms cannot be installed between the legs of the landing gear due to their size. However, this configuration protects the upper arms against crashes as long as the landing gear is extended. In any case, the frame of the shoulder was placed as close as possible to the center of mass of the multirotor in order to reduce the mass unbalance.

As mentioned before, this work exploits the symmetry in the aerial manipulation system for compensating the torque generated by the arms. Consider the right side of Figure 1. If the shoulder pitch and elbow pitch joints of both arms move in the same direction, but the shoulder yaw joints move in different directions, then the torque generated by the left arm is cancelled by the torque generated by the right arm around the roll and yaw angles, although at expenses of increasing the reaction torque in the pitch angle.

C. Electronics

The electronics, placed in the central hub of the vehicle, consists of an Odroid U3 computer board where the motion control and data acquisition program is executed, a STM32F3 Discovery board for obtaining the accelerometer, gyroscope and magnetometer measurements, and a USB WiFi module for communication with the ground control station. These devices

are powered from a 2S 2200 mAh LiPo battery through a 5V 1.5A Recom voltage regulator. Two USB-to-UART modules connect the Odroid board with the servo actuators and with the Discovery board for controlling the arms and for obtaining the measurements. A block diagram with the different subsystems, components and architecture is represented in Figure 3.In this implementation, for simplicity, the Odroid and the autopilot are not connected as the control of the arms is independent.

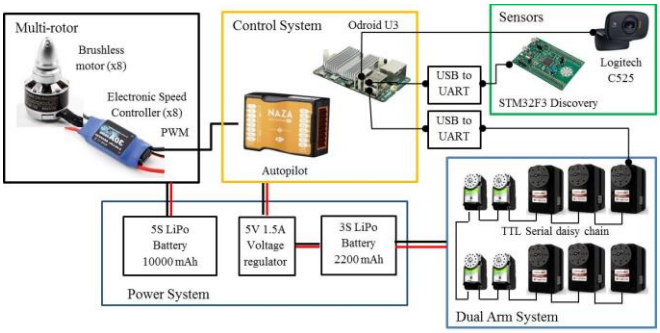

Figure 3. Hardware architecture of the dual arm aerial manipulator.

III. Aerial Manipulator Modeling and Control

A. Modelling

The dynamic behavior of an aerial manipulation system consisting in an aerial platform with one or multiple robotic arms suffers from variations in the mass distributions. This implies that the moments of inertia change significantly and the system center of mass moves continuously, introducing reaction forces and torques which compromise the stability of the aerial platform [15]. It results convenient in this kind of systems to formulate the equations of motion with respect to its center of mass [16].

Figure 4 shows a multirotor platform equipped with two robotic arms with multiple joints. Although the kinematic and dynamic model described here can be applied to an arbitrary number of joints, the notation and equations are particularized to the case of a dual arm manipulator with three joints for end effector positioning. The wrist joints are not considered in this analysis as the moment of inertia of the associated links is much lower than the positioning joints. All joints are revolute and provide a single degree of freedom. Therefore, considering the 6 DOF associated to the position and attitude of the aerial platform, the whole system will have $D = 12$ DOF.

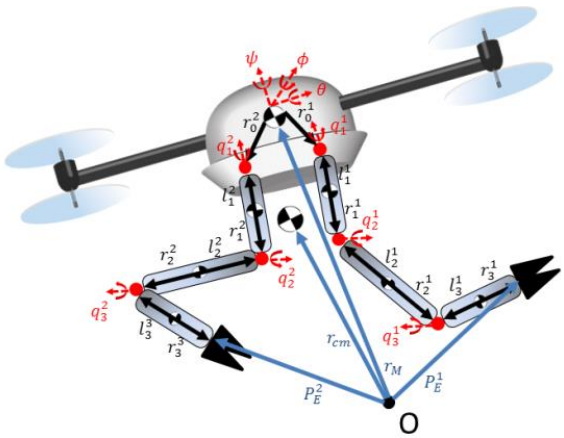

Figure 4. A multirotor equipped with two robotic arms.

The dynamic model of this system can be derived from the Lagrange's equations. The vector of generalized coordinates is defined as $\boldsymbol{\xi} = [\boldsymbol{r_{cm}}, \boldsymbol{\eta}, \boldsymbol{q^1}, \boldsymbol{q^2}]^T \in \mathbb{R}^{12}$, where $\boldsymbol{r_{cm}}$ represents the center of mass of the whole system, $\boldsymbol{\eta} = [\phi, \theta, \psi]^T \in \mathbb{R}^3$ is the vehicle attitude by the roll, pitch, yaw Euler angles, and $\boldsymbol{q^i} = \left[q_1^i\ q_2^i\ q_3^i\right]^T \in \mathbb{R}^3 (i = 1, 2)$ are the joint angles of the i-th arm. The equations of motion are derived from the general Lagrange formulation:

$$\frac{d}{dt}\frac{\partial L}{\partial \dot{\xi}} - \frac{\partial L}{\partial \xi} = \boldsymbol{F} \tag{1}$$

where $\boldsymbol{F} \in \mathbb{R}^{12}$ is the generalized force/torque vector that includes the torque generated by the propellers and the torque of each joint in the arms. The Lagrangian L is defined as the difference between the kinetic and potential energy of the system K and V, functions of the generalized coordinates:

$$L(\boldsymbol{\xi}, \dot{\boldsymbol{\xi}}) = K_T(\boldsymbol{\xi}, \dot{\boldsymbol{\xi}}) + K_R(\boldsymbol{\xi}, \dot{\boldsymbol{\xi}}) - V(\boldsymbol{\xi}) \tag{2}$$

The translational kinetic energy of the system is given by:

$$K_T = \frac{1}{2} M_T \dot{\boldsymbol{r}}_{\boldsymbol{cm}}^{\boldsymbol{T}} \dot{\boldsymbol{r}}_{\boldsymbol{cm}} \tag{3}$$

where M_T is the total mass of the system and $\dot{\boldsymbol{r}}_{\boldsymbol{cm}} \in \mathbb{R}^3$ is the velocity of the system center of mass (CM), given by:

$$\boldsymbol{r_{cm}} = \frac{1}{M_T}\left(\boldsymbol{r_M} m_0 + \sum_{p=1}^{2}\sum_{j=1}^{3} \boldsymbol{d_j^p} m_j^p\right) \tag{4a}$$

$$\boldsymbol{d_j^i} = \boldsymbol{r_M} + T_0 \sum_{p=1}^{j} (\boldsymbol{R_{0,p-1}^i r_{p-1}^i} - \boldsymbol{R_{0,p}^i l_p^i}) \tag{4b}$$

Here m_0 is the mass of the aerial platform, $\boldsymbol{r_M}$ denotes the position vector of the system CM w.r.t. the inertial frame, r_p^i and l_p^i are defined in Figure 4, and $R_{0,0}^i$ is the identity matrix. The rotational kinetic energy of the system is given by:

$$K_R = \frac{1}{2}\sum_{i=1}^{2}\sum_{k=0}^{3} \{\boldsymbol{\omega_k^i}\, \boldsymbol{I_k^i \omega_k^i} + m_k^i\, \boldsymbol{\dot{\rho}_k^i \dot{\rho}_k^i}\} \tag{5}$$

$$\boldsymbol{\dot{\rho}_k^i} = \sum_{p=1}^{2}\sum_{j=0}^{3} \boldsymbol{\omega_j^p} \times \boldsymbol{v_{j(k\delta_{ip})}^p} \in \mathbb{R}^3 \tag{6}$$

$$\boldsymbol{\omega_k^i} = \boldsymbol{\omega_0} + \boldsymbol{T_0 T_k^i \dot{q}^i} \in \mathbb{R}^3 \tag{7}$$

$$T_k^i = \left[R_{0,1}^i u_1^i, R_{0,2}^i u_2^i, \ldots, R_{0,k}^i u_k^i, 0, \ldots, 0\right] \in \mathbb{R}^{3\times 3} \tag{8}$$

Here $\boldsymbol{\omega_0^p} = \boldsymbol{\omega_0}$ $(p = 1,2,3)$ is the angular velocity of the multirotor referred to the inertial frame, while $\dot{\boldsymbol{q}}^{\boldsymbol{i}}$ represents the joint rates of the i-th manipulator. The terms $\boldsymbol{u_j^i} \in \mathbb{R}^3$ are unit column vectors denoting the rotation axis of the j-th joint of the i-th manipulator, and I_k^i is the inertia of each link. The terms $\boldsymbol{v_{jk}^i} \in \mathbb{R}^3$ in Equation (6) are the barycentric vectors [16], defined as the position vector of the k-th link CM of manipulator i with respect to the system CM. The calculation of these terms is detailed in [16].

The potential energy due to gravity is calculated with respect to the system center of mass:

$$V = -\boldsymbol{g} M_T z_{cm} \tag{9}$$

where $\boldsymbol{g} = [0, 0, -9.81]^T$ is the gravity vector and z_{cm} is the position of the center of mass in the Z-axis. The equation of motion of the system is the expressed in the general form:

$$\boldsymbol{M}(\boldsymbol{r})\ddot{\boldsymbol{\xi}} + \boldsymbol{C}(\boldsymbol{r}, \dot{\boldsymbol{r}})\dot{\boldsymbol{\xi}} + \boldsymbol{G}(\boldsymbol{\xi}) = \boldsymbol{\mathcal{F}_T} \quad (10)$$

Here $\boldsymbol{M} \in \mathbb{R}^{D\times D}$, $\boldsymbol{C} \in \mathbb{R}^{D}$and $\boldsymbol{G} \in \mathbb{R}^{D}$ are respectively the inertia matrix, the centrifugal and Coriolis terms, and the gravitational force term. Vector $\boldsymbol{r} = [\boldsymbol{\eta}, \boldsymbol{q^1}, \boldsymbol{q^2}]^T$ represents the multirotor rotation and the manipulators' joint angles. It can be demonstrated that the inertia matrix resulting for the developed dual arm aerial manipulation system has the following form:

$$\boldsymbol{M}(\boldsymbol{r}) = \begin{bmatrix} \boldsymbol{I_3 M_T} & \boldsymbol{0} & \boldsymbol{0} & \boldsymbol{0} \\ \boldsymbol{0} & \boldsymbol{M_\eta}(\boldsymbol{r}) & \boldsymbol{M_{\eta q1}}(\boldsymbol{r}) & \boldsymbol{M_{\eta q2}}(\boldsymbol{r}) \\ \boldsymbol{0} & \boldsymbol{M^T_{\eta q1}}(\boldsymbol{r}) & \boldsymbol{M_{q1}}(\boldsymbol{r}) & \boldsymbol{M_{q1q2}}(\boldsymbol{r}) \\ \boldsymbol{0} & \boldsymbol{M^T_{\eta q2}}(\boldsymbol{r}) & \boldsymbol{M^T_{q1q2}}(\boldsymbol{r}) & \boldsymbol{M_{q2}}(\boldsymbol{r}) \end{bmatrix} \quad (11)$$

Several model-based controllers can be implemented using this dynamic model. Nevertheless, the manufacture of a low weight manipulator involves the use of commercially available servo actuators that do not provide any joint torque, velocity or acceleration feedback, which may be a problem for the practical implementation of many controllers. In order to cope with this limitation, a method for estimating servo acceleration and the torque that the manipulator exerts over the platform based on the dynamic model is described in Section IV.

B. Control

One of the main purposes of this paper is to highlight the importance of, on one hand, minimizing total reaction torques generated by the arms, and on the other hand, of having a good estimation of these torques in such a way that the controller can compensate them. In this work a nonlinear controller based on integral backstepping [25] is proposed, adapted to the dual-arm configuration. The expression of the attitude controller for a multirotor equipped with a dual-arm is given by:

$$\boldsymbol{U_\eta} = \boldsymbol{M_\eta^{-1}}\left[\boldsymbol{K_1 e_\eta} + \boldsymbol{K_2 e_{\dot\eta}} + \boldsymbol{K_3 \chi_\eta}\right] + \boldsymbol{C_\eta} + \boldsymbol{G_\eta} + \widetilde{\boldsymbol{M}}_{\boldsymbol{\eta q}} \quad (12)$$

Here $\boldsymbol{U_\eta}$ is control signal applied to the propellers (thrust and roll, pitch and yaw torques), while $\widetilde{\boldsymbol{M}}_{\boldsymbol{\eta q}}$ is defined as:

$$\widetilde{\boldsymbol{M}}_{\boldsymbol{\eta q}} = [\boldsymbol{M_{\eta q1}}(\boldsymbol{r}) \quad \boldsymbol{M_{\eta q2}}(\boldsymbol{r})] \begin{bmatrix} \ddot{\boldsymbol{q}}^{\boldsymbol{1}} \\ \ddot{\boldsymbol{q}}^{\boldsymbol{2}} \end{bmatrix} \in \mathbb{R}^3 \quad (13)$$

The gravity, Coriolis and inertia terms in Equation (12) can be computed from the equations of the dynamic model and the measurements provided by the IMU and the servos. The tracking error $\boldsymbol{e_\eta}$, its integral $\boldsymbol{\chi_\eta}$ and the angular velocity tracking error, $\boldsymbol{e_{\dot\eta}}$ are defined in the following way:

$$\boldsymbol{e_\eta} = \boldsymbol{\eta_d} - \boldsymbol{\eta} \in \mathbb{R}^3 \quad (14)$$

$$\boldsymbol{\chi_\eta} = \int_0^t \boldsymbol{e_\eta}(t)dt \in \mathbb{R}^3 \quad (15)$$

$$\boldsymbol{e_{\dot\eta}} = \boldsymbol{k_\eta e_\eta} + \boldsymbol{\lambda_\eta \chi_\eta} + \dot{\boldsymbol{\eta}}_{\boldsymbol{d}} - \dot{\boldsymbol{\eta}} \in \mathbb{R}^3 \quad (16)$$

$$\boldsymbol{K_1} = \mathbb{I}_3 - \boldsymbol{\lambda_\eta^2} + \boldsymbol{k_\eta} \in \mathbb{R}^{3\times3} \quad (17)$$

$$\boldsymbol{K_2} = \boldsymbol{k_\eta} + \boldsymbol{k_{\dot\eta}} \in \mathbb{R}^{3\times3} \quad (18)$$

$$\boldsymbol{K_3} = -\boldsymbol{k_\eta \lambda_\eta} \in \mathbb{R}^{3\times3} \quad (19)$$

Here $\mathbf{k_\eta}$, $\mathbf{k_{\dot\eta}}$ and $\boldsymbol{\lambda_\eta}$ are positive diagonal controller matrix gain. The vectors $\boldsymbol{C_\eta} \in \mathbb{R}^3$ and $\boldsymbol{G_\eta} \in \mathbb{R}^3$ are the lower part of the Coriolis and centrifugal force and gravity force vectors, respectively. The controller derivation and stability proof is omitted here and can be found in [25].

In the expression of the controller given by Equation (12), the term $\widetilde{\boldsymbol{M}}_{\boldsymbol{\eta q}}$ compensates the reaction torques of the arms, making use of their dynamic model. Having a good estimation of the angular accelerations of the joints of both arms is very important since errors in the accelerations measured can cause a poor performance for the controller, as will be shown with simulations in Section V.

IV. Torque Estimation

A. Technological Limitations of Servo Actuators

Smart servos such as Herkulex or Dynamixel are well suited for building very low weight robotic arms intended for aerial manipulation due to their high torque to weight ratio (7.6 N·m/0.145 Kg for the Herkulex DRS-0602) and because they integrate all the mechatronics in a compact size device, simplifying significantly the mechanical design. However, as mentioned at the end of Section III-A, there are several important limitations in their application that affect to the implementation of control methods in terms of update time, control capabilities and available feedback. These servos are designed to be connected in daisy chain, sharing the same TTL bus between multiple servos. Therefore, as the number of devices increases, the maximum update rate decreases. In the case of the six actuators needed for the positioning of the dual arm, the update time was set to 30 ms to ensure low packet loss. Identification experiments with a single servo has shown that the maximum control/feedback rate is around 100 Hz, far away from the 1 KHz rate used in torque control. The signals of interest provided by the servos include the position, differential position (speed estimation), and PWM signal. As mentioned above, no acceleration or torque feedback is provided in commercial servos used in lightweight arms. Joint torque could be inferred from the PWM signal, although a good model for the friction is needed. Finally, it is necessary to remark that the only way to control the servo is specifying the desired goal position and the play time, that is, the time required for reaching the reference. The embedded servo controller generates then a trapezoidal velocity profile for satisfying these two motion constraints, although there is no direct control over joint speed or acceleration.

B. Structure of the Torque Estimator

In order to analyze how arms motion affects the stability of the aerial platform, a torque estimation system which exploits the information provided by the Herkulex servos has been developed. This work considers only the influence of the shoulder and elbow servos, which determine the position of the end effector, neglecting the torque generated by the wrist actuators for the reason indicated in Section III-A. The block diagram of the estimator can be seen in Figure 5, while Figure 6 shows its application in the control system. The controller embedded on all the servos generates a trapezoidal velocity profile for reaching the reference position in the specified motion time. The shoulder and elbow servos provide position

and velocity (differential position) feedback that is taken as input by the Phase Lock Loop (PLL) acceleration estimator. The position, velocity and acceleration estimations of each joint are passed to the dynamics equations of the aerial manipulation system (Section III) implemented in MATLAB-Simulink for obtaining the three components of the torque generated by the arms (inertia τ_M, Coriolis τ_C and gravity τ_G) w.r.t. the center of mass of the whole system. Identifying separately these terms it is possible to analyze their relative influence over the stability of the aerial platform.

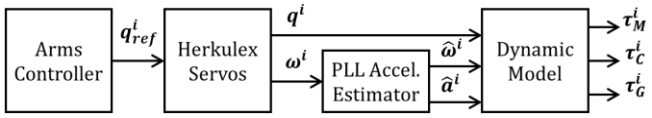

Figure 5. Block diagram of the torque estimator.

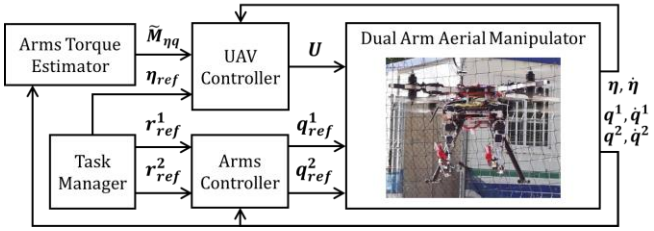

Figure 6. Block diagram of the control system with arms torque estimation.

In the control scheme depicted in Figure 6, the sampling rate of the UAV controller will be typically higher (≥100 Hz) than the rate of the arms torque estimator (<50 Hz) due to the limitations of the controller embedded in the servo actuators, which may affect to the derivative terms in the controller.

C. Payload Estimation

Although the duty cycle of the PWM signal provided by the servos is not accurate and reliable enough for estimating the joint torque, it may be useful for estimating the weight of a grasped object in static conditions. A similar idea was proposed in [21] motivated by the convenience of tuning online the UAV and arms controller according to the mass of the payload. Assuming for simplicity that the estimation is done with the shoulder pitch joint while the elbow joint is fully stretched, the torque due to gravity that the shoulder pitch joint must support when holding an object is:

$$\tau^i_{2,G} = sin\left(q^i_2\right) \cdot g \cdot [L^i \cdot m_L + l^i_a \cdot m^i_a] \qquad (20)$$

In this equation, $\tau^i_{2,G}$ is the gravity term in the shoudler pitch joint of the i-th arm, g is the gravity constant, L and l^i_a are the distances from this joint to the grasped object and to the CoM of the arm, respectively, while m_L and m^i_a are the masses of the load and the mass of the arm itself. Considering that the joint torque is proportional to the duty cycle:

$$\tau^i_{2,G} = pwm^i_2 \cdot \tau^i_{2,stall} \quad , \quad pwm^i_2 \in [0,1] \qquad (21)$$

where $\tau^i_{2,stall}$ is the stall torque of the shoulder pitch servo, and neglecting the effect of static frictions in the servo, then the weight of the load can be obtained from Equation (20).

V. Results

A. Servo Joint State Estimation

The proposed method for estimating servo acceleration based on PLL described in Section IV-B is evaluated here. Figure 7 shows the measured and reference position along with the estimated velocity and acceleration of the shoulder pitch servo when it is requested to move from 0 to 90 deg and from 90 to 0 deg in one second. A 0.5 Kg payload was attached to the wrist point, with the forearm extended. The servo provides measurements at 30 Hz.

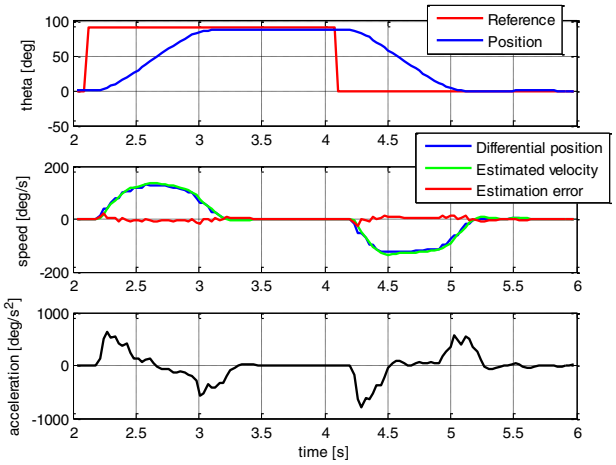

Figure 7. Position, velocity and estimated acceleration for the shoulder pitch servo moving from 0 to 90 [deg] and from 90 to 0 [deg] in one second.

The torque introduced in the base of the multi-rotor when the left arm executes the motion described in Figure 7 (90 deg step in the shoulder pitch, with the forearm extended and no load at the wrist point) is represented in Figure 8. The inertia, Coriolis and gravity terms can be identified separately for the three axes. Note that the gravity term is dominant in the pitch angle, while the inertia and Coriolis terms in the roll and yaw angles are associated to the unbalance in the mass as there is no compensation with the right arm.

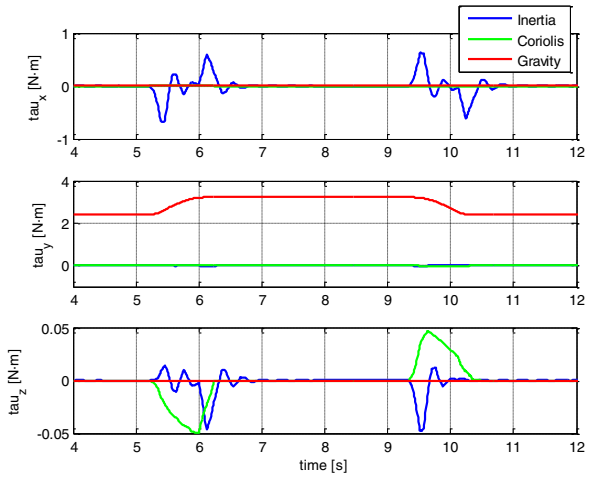

Figure 8. Inertia (blue), Coriolis and centrifugal (green) and gravity terms (red) in the XYZ axes for the 90 deg step in the non-compensated (only left arm motion) shoulder pitch joint.

B. *Simulations*

A MATLAB/Simulink simulator has been developed for analyzing how the performance of the position controller of the UAV is improved when the torque estimation is considered in the backstepping controller, that is, when the term $\widetilde{\boldsymbol{M}}_{\boldsymbol{\eta q}}$ is introduced. Figure 9 compares the magnitude of the position error of the multirotor when it is in hover state in two cases: with and without torque estimation. Note that, although the error in the worst case is not too high due to the low mass and inertia of the arms, the controller is improved. The simulator implements the dynamic model described in Section III-A, no addition effects like motor dynamics or noise are considered.

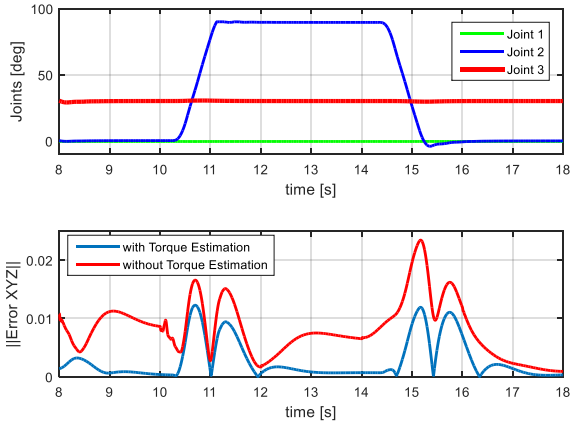

Figure 9. Shoulder pitch joint position of the left arm (up) and magnitude of the Cartesian position error of the multirotor with and without torque estimation (down) with backstepping control.

C. *Motion Coordination for Torque Cancellation*

The intention of this experiment is demonstrating how the motion of the arms can be coordinated in such a way that the torque disturbance in the roll and yaw angles is cancelled, at expenses of increasing the perturbation over the pitch angle. The experiment was conducted in a test-bench so this effect is appreciated more clearly, hanging the aerial manipulator from wires for emulating hovering conditions. Otherwise the vibrations generated by the propellers and the actuation of the autopilot would introduce undesired effects. The manipulator executes an extension-contraction motion in which the left (right) arm is initially retracted, extends to the left (right) side rotating around the shoulder yaw joint, and goes back to the initial position. As seen in Figure 10, the oscillation in the roll-yaw angles is more significant when the motion of the arms is asymmetric w.r.t. the symmetric motion case.

D. *Payload Estimation*

The proposed method for estimating the mass of a grasped object based on the PWM signal described in Section IV-C is evaluated here. In this experiment, different payloads were attached at the wrist point of the left arm at $L = 0.5\ [m]$ distance from the shoulder pitch joint. The elbow pitch angle was fixed to its minimum value $q_3^1 = 10\ [deg]$. The mass of the arm obtained from the 3D model is $m_a^1 = 0.38\ [Kg]$, with its CoM at $l_a^1 = 0.21\ [m]$ from the shoulder pitch joint. The shoulder pitch joint angle was incremented in $10\ [deg]$ steps up to $90\ [deg]$. Figure 11 shows the duty cycle in this joint for different payloads and measurement angles. The no-load case (black line) corresponds to the case in which the arm lifts its own weight.

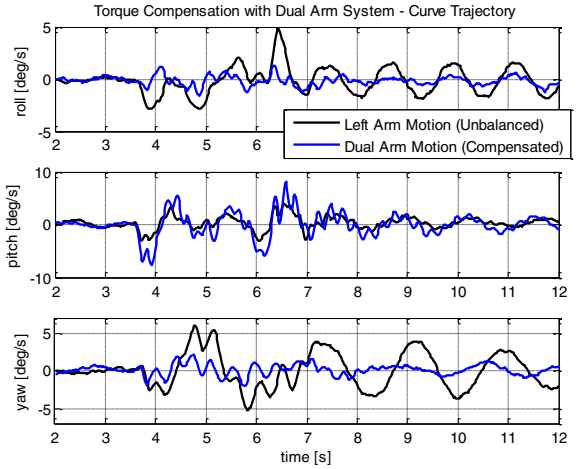

Figure 10. RPY rate [deg/s] in the curve trajectory experiment with left arm motion (unbalanced) and with dual arm motion (torque compensation).

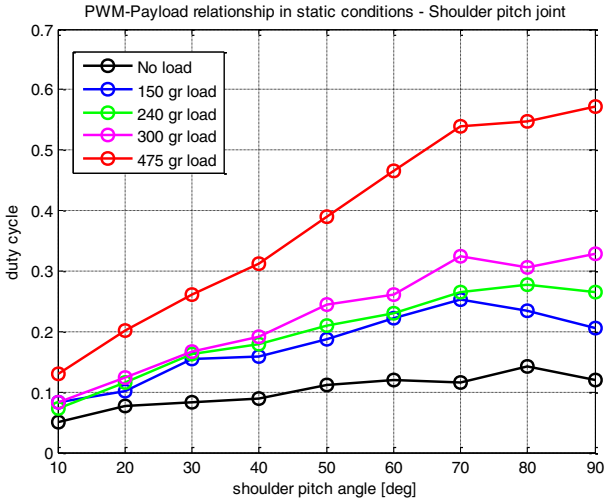

Figure 11. Duty cycle of the shoulder pitch joint for different grasped payloads and reference angles.

E. *Flight Tests*

Preliminary flight tests have been conducted in outdoors for analyzing qualitatively the influence of arms motion over the multirotor controller, implemented with a Naza autopilot. The experiments consisted in the execution of different trajectories with the arms while the UAV stayed in hovering at two meters height. No height sensor was employed, so a human pilot had to correct height deviations. Two 0.21 Kg pliers were attached at the writ point of both arms for increasing the inertia. For safety reasons, a net was deployed covering a volume of 5×5×4 m.

A sequence of images of the aerial manipulator on flight while it was executing the trajectories described in previous subsection can be seen in Figure 12. It was found during the realization of the experiments that the aerial platform was more affected by the wind than by the motion of the arms. This is so because the inertia of the arms is relatively low with respecto to the inertia of the aerial platform.

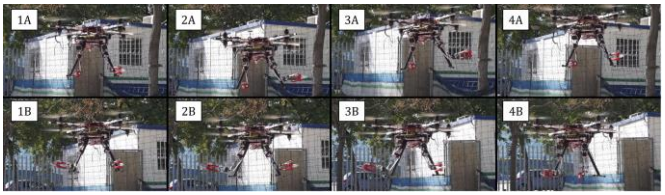

Figure 12. Outdoor flight test. Asymmetric motion with the left arm (A), and symmetric trajectory with both arms (B). This disturbance is more significant in the first case due to mass unbalance. Two 0.2 Kg pliers were attached at the tip of each arm for increasing the inertia.

VI. CONCLUSION

This paper has presented the design of a dual arm aerial manipulation robot consisting in two human-size and ultra-lightweight (1.8 Kg) arm prototypes integrated in an octorotor platform. Each arm provides three degrees of freedom for end-effector positioning and two DOF for wrist orientation. Due to the lack of torque/acceleration feedback or control capabilities (which most model-based controllers assume to be available) in the servos typically employed for building low weight arms, the paper proposes the design of a torque estimator that computes the reaction torques that the arms exert over the UAV. A control scheme that makes use of this estimator is described and evaluated in simulation. The symmetry of the dual arm manipulator is also exploited for reducing the perturbation over the controller, coordinating the motion of the arms in such a way that the torque induced in the roll and yaw angles by one arm is cancelled with the other, at the expenses of increasing the perturbation introduced in the pitch angle. Preliminary flight tests have been conducted in outdoors for analyzing qualitatively the influence of arms motion over the attitude/position of an octo-rotor platform controlled with a commercial autopilot.

ACKNOWLEDGMENT

This work has been funded by the Spanish MINECO Retos project AEROMAIN (DPI2014-5983-C2-1-R) and by the H2020 AEROARMS (AErial RObotic system integrating multiple ARMS and advanced manipulation capabilities for inspection and maintenance) Project, Grant Agreement Nº 644271. The research activity of Alejandro Suarez is supported by the Spanish Ministerio de Educacion, Cultura y Deporte FPU Program.

REFERENCES

[1] Kondak, K., Krieger, K., Albu-Schaeffer, A., Schwarzbach, M., Laiacker, M., Maza, I., ... & Ollero, A. (2013). Closed-loop behavior of an autonomous helicopter equipped with a robotic arm for aerial manipulation tasks. Inter. Journal of Advanced Robotic Systems, 10.

[2] Jimenez-Cano, A. E., Martin, J., Heredia, G., Ollero, A., & Cano, R. (2013, May). Control of an aerial robot with multi-link arm for assembly tasks. In Robotics and Automation (ICRA), 2013 IEEE International Conference on (pp. 4916-4921). IEEE.

[3] Arleo, G., Caccavale, F., Muscio, G., & Pierri, F. Control of quadrotor aerial vehicles equipped with a robotic arm. In Control & Automation (MED), 2013 Mediterranean Conf. on (pp. 1174-1180).

[4] Caccavale, F., Giglio, G., Muscio, G., & Pierri, F. (2014). Adaptive control for UAVs equipped with a robotic arm. Jeb, 3, I3.

[5] Ruggiero, F., Trujillo, M. A., Cano, R., Ascorbe, H., Viguria, A., Peréz, C., ... & Siciliano, B. A multilayer control for multirotor UAVs equipped with a servo robot arm. In Robotics and Automation (ICRA), 2015 IEEE International Conference on (pp. 4014-4020).

[6] Pounds, P. E., Dollar, A. M. (2014). Aerial grasping from a helicopter UAV platform. In Experimental Robotics (pp. 269-283). Springer.

[7] Orsag, M., Korpela, C., Bogdan, S., & Oh, P. (2014, May). Valve turning using a dual-arm aerial manipulator. In Unmanned Aircraft Systems (ICUAS), 2014 Int. Conference on (pp. 836-841). IEEE.

[8] Kondak, K., Ollero, A., Maza, I., Krieger, K., Albu-Schaeffer, A., Schwarzbach, M., & Laiacker, M. (2015). Unmanned Aerial Systems Physically Interacting with the Environment: Load Transportation, Deployment, and Aerial Manipulation. In Handbook of Unmanned Aerial Vehicles (pp. 2755-2785). Springer Netherlands.

[9] B. Yuksel, C. Secchi, H. Bulthoff, A. Franchi. A nonlinear force observer for quadrotors and application to physical interactive tasks. 2014 IEEE/ASME Int. Conf. on Advanced Intelligent Mechatronics, Jul 2014, Besancon, France.

[10] Bellens , S., De Schutter, J., & Bruyninckx, H., A hybrid pose/ wrench control framework for quadrotor helicopters, In Proc. of the ICRA 2012, Saint Paul, USA.

[11] Ruggiero, F., Cacace, J., Sadeghian, H., & Lippiello, V. (2015). Passivity-based control of VToL UAVs with a momentum-based estimator of external wrench and unmodeled dynamics. Robotics and Autonomous Systems, 72, 139-151.

[12] Ruggiero, F., Cacace, J., Sadeghian, H., & Lippiello, V. (2014, May). Impedance control of VTOL UAVs with a momentum-based external generalized forces estimator. In Robotics and Automation (ICRA), 2014 IEEE International Conference on (pp. 2093-2099). IEEE.

[13] Yoshida, K., Kurazume, R., & Umetani, Y. Dual arm coordination in space free-flying robot. In Robotics and Automation, 1991. Proceedings. 1991 IEEE Int. Conference on (pp. 2516-2521).

[14] Yoshida, K., Kurazume, R., & Umetani, Y. Torque optimization control in space robots with a redundant arm. In Intelligent Robots and Systems' 91.'Intelligence for Mechanical Systems, Proceedings IROS'91. IEEE/RSJ International Workshop on (pp. 1647-1652).

[15] E. Papadopoulos and A. Moosavian. Dynamics and control of space free-flyers with multiple manipulators. Advanced robotics 9.6 1994, pp. 603-624.

[16] E. Papadopoulos. On the dynamics and control of space manipulators. Diss. Massachusetts Institute of Technology, 1990

[17] Orsag, M., Korpela, C., & Oh, P. (2013). Modeling and control of MM-UAV: mobile manipulating unmanned aerial vehicle. Journal of Int. & Robotics Systems 69 (1-4) 227-240.

[18] Kondak, K., Huber, F., Schwarzbach, M., Laiacker, M., Sommer, D., Bejar, M., & Ollero, A. (2014, May). Aerial manipulation robot composed of an autonomous helicopter and a 7 degrees of freedom industrial manipulator. In Robotics and Automation (ICRA), 2014 IEEE International Conference on (pp. 2107-2112). IEEE.

[19] Cano, R., Pérez, C., Pruano, F., Ollero, A., & Heredia, G. (2013). Mechanical design of a 6-DOF aerial manipulator for assembling bar structures using UAVs. In 2nd RED-UAS 2013 Workshop on Research, Education and Development of Unmanned Aerial Systems.

[20] Bellicoso, C. D., Buonocore, L. R., Lippiello, V., & Siciliano, B. (2015, June). Design, modeling and control of a 5-DoF light-weight robot arm for aerial manipulation. In Control and Automation (MED), 2015 23th Mediterranean Conference on (pp. 853-858). IEEE.

[21] Suarez, A., Heredia, G., & Ollero, A. Lightweight compliant arm for aerial manipulation. In Intelligent Robots and Systems (IROS), 2015 IEEE/RSJ International Conference on (pp. 1627-1632). IEEE.

[22] Suarez, A., Heredia, G. & Ollero, A. Lightweight compliant arm with compliant finger for aerial manipulation and inspection. In Intelligent Robots and Systems (IROS) 2016 IEEE/RSJ Int. Conference on.

[23] https://www.prodrone.jp/en/archives/1420/

[24] https://www.youtube.com/watch?v=ZxRlwf7cXQ8

[25] Jimenez-Cano, A. E., J., Heredia, G., & Ollero, A. (2015, September). Aerial manipulator for structure inspection by contact from the underside. In Intelligent Robots and Systems (IROS), 2015 IEEE/RSJ International Conference on (pp. 1879-1884). IEEE.